Collisional heating and adiabatic expansion of warm dense matter with intense relativistic electrons

J. E. Coleman* and J. Colgan
Los Alamos National Laboratory, Los Alamos, New Mexico 87545, USA
(Received 11 April 2017; published 13 July 2017)

Adiabatic expansion of a warm dense Ti plasma has been observed after isochoric heating of a 100-μm-thick Ti foil with an ∼100-ns-long intense relativistic electron bunch at an energy of 19.8 MeV and a current of 1.7 kA. The expansion fits well with the analytical point-source solution. After 10 J is deposited and the plasma rapidly expands out of the warm dense phase, a stable degenerate plasma ($T \sim 1.2$ eV) with $n_e > 10^{17}$ cm^{-3} is measured for >100 ns. This is the first temporal measurement of the generation and adiabatic expansion of a large volume (3×10^{-4} cm^3) of warm dense plasma isochorically heated by intense monochromatic electrons. The suite of diagnostics is presented, which includes time-resolved plasma plume expansion measurements on a single shot, visible spectroscopy measurements of the emission and absorption spectrum, measurements of the beam distribution, and plans for the future.

DOI: 10.1103/PhysRevE.96.013208

I. INTRODUCTION

Warm dense matter (WDM) is a region in temperature-density space in the range of $0.1 < T_e$ (eV) < 10 eV and $10^{22} < n_e$ (cm^{-3}) $< 10^{24}$ for most metals that is not described well by normal condensed matter or weakly coupled plasma theory. WDM has been produced by multiple mechanisms through shock-heating with photons, magnetic compression, or collisional heating with particle beams. High-power lasers with 6-ns pulses of 300–450 J were used to shock-heat 300 μm of LiH to 2 eV, 10^{23} cm^{-3} [1,2], and a stepped 13.5-kJ, 3-ns pulse profile was used to shock-heat a 70-μm CH shell to 8 eV, 10^{24} cm^{-3} [3]. Free electron lasers have been explored as heating probes also; the LCLS 8.9-keV, 60-fs x-ray free electron laser provided 1 mJ of heat to 0.5 μm of Ag to achieve 10 eV and calculated densities of 10^{24} cm^{-3} with two equation-of-state (EOS) models [4]. The FLASH UV free electron laser delivered 10–30 μJ in 25 fs to a 20-μm spot to heat Al to 0.8 eV [5]. Laser-heating experiments have traditionally been used to validate the Hugoniot curves [6].

Magnetic compression produced shock-heating with both *Z* and *X* pinches. The x-ray Thomson measurements on the *Z* facility indicate shock compression at 20 MA of carbon foams to a temperature of 4.3 eV and $n_e \sim 10^{20}$ cm^{-3} [7]. A two-wire *X* pinch drove 40 μm of Al with 150 kA to produce 10- to 30-eV coronal plasmas with $n_e < 10^{20}$ cm^{-3} [8]. These measured densities were slightly below those of the warm dense phase.

Particle-beam-driven WDM has been investigated by several means. Research with uranium ions at GSI has proposed collisional heating by delivering 5×10^{11} U^{28+} ions accelerated to 400 MeV/u (95.2 GeV) in a 350-μm spot and 70-ns pulse to achieve 4.2-eV temperatures in solid hydrogen [9,10]. It demonstrated heating of a 100-μm-thick W target to 0.56 eV with U^{74+} ions accelerated to 350 MeV/u (83.3 GeV) in a 120-ns bunch [11]. Intense light ions from the NDCX-I facility [12] have been used to heat Au targets to 0.38 eV [13] and 0.27 eV [14] using a 4-μs bunch of 0.3-MeV, 30-mA K^+ ions; no density was measured in either case. The NDCX-II accelerator provided 1.2-MeV Li^+ ions with 1.6 nC of charge in a 2-ns pulse [15] and, more recently, 15 nC of He^+ ions [16] has been used to begin heating experiments on 300-nm-thick Sn [17]. None of these experiments have successfully measured a density or an expansion rate.

Intense short-pulsed lasers have also been used to accelerate ions. A 60-J, 1-ps laser heated a 20-μm-thick Au foil to produce 60-nC protons, with a peak energy of 17 MeV, which deposited 180 mJ in C, heating it to 0.39 eV [18]. The 80-J, 650-fs Trident laser accelerated ∼140-MeV Al^+ ions from 110-nm-thick Al foil onto a 10-μm-thick Au and 15-μm-thick C hybrid interface. Expansion speeds of 6.7 and 7.5 μm/ns were measured for C and Au, leading to inferred temperatures of 1.7 and 5.5 eV [19,20] using the RAGE code [21] and available SESAME tables [22]. Again, these experiments did not measure a plasma density. To date there has been no measurement of plasma density from collisional, isochoric heating of a solid target.

Intense relativistic electron beam-target interactions were studied nearly two decades ago. The interactions of intense electrons with plasma densities exceeding the beam density [23–25] led to the development of Wakefield acceleration techniques for bunches < 100 ps. Experiments explored time-dependent focusing effects through streaked measurements of Cherenkov light produced by the beam at focus [26]. Simple gated images of the plasma plume were made at the ETA facility but were not quantitatively characterized [27]. LSP was used to investigate the beam-target interaction [28,29] by characterizing the gas desorption of the contaminant layer and the backstreaming velocity using particle-in-cell techniques; dense plasmas and hydro motion were not considered at the time. A detailed model of the hydrodynamic expansion of the particle-beam-heated foil has been attempted with the hydro codes LASNEX [27,30] and, more recently, RAGE [21,31], in addition to a particle-in-cell–fluid hybrid model in LSP[32]. The integration of these codes is still in the development stage in order to properly deposit the particle beam energy and simultaneously model the hydro motion, so no results are presented.

*josh.e.coleman@gmail.com

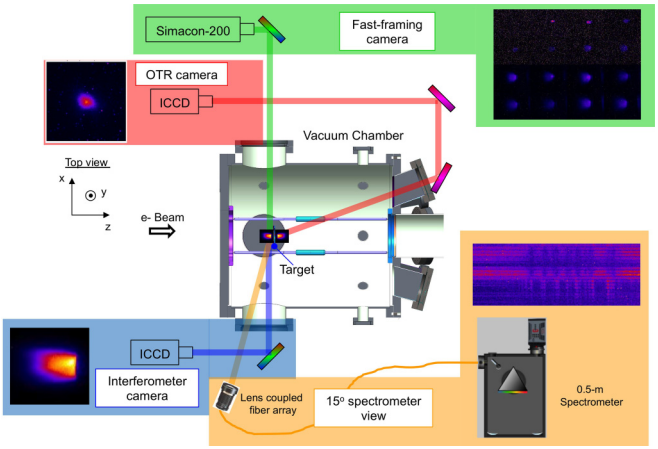

FIG. 1. View of the vacuum test section in which the expanding warm dense plasma is diagnosed. The target location, optical diagnostic layouts, lines of sight, and sample data sets are shown. The imaging station for OTR is shown in red; the imaging station for the interferometer camera, in blue; the fast-framing camera, in green; and the 15° upstream spectrometer, in orange. (The orthogonal visible spectrometer is not shown).

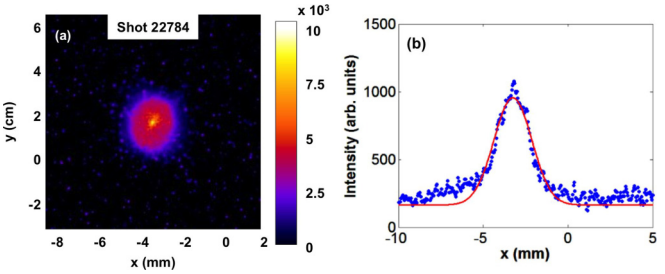

FIG. 2. (a) A 10-ns gated OTR image of the beam distribution on the foil, 20 ns after the beginning of the pulse. (b) Integrated intensity and Gaussian fit of the OTR image. Note the enhancement at the peak.

An electron linear induction accelerator [33,34] is used to produce a large volume (3×10^{-4} cm^3) of WDM that expands adiabatically, which has the potential to provide a longer, stable method of measuring the EOS. We are not claiming this in the present paper. There are three parameters we plan to measure for the EOS: temperature, density, and pressure. A 100-ns-long, 1.7-kA electron bunch is accelerated and transported through the induction linac to 19.8 MeV and then is focused onto a 100-μm-thick Ti foil. The optical diagnostic suite (Fig. 1), including plume imaging, near-field optical transition radiation (OTR) [35–39], and visible spectroscopy both orthogonal to the surface and on the target face, is presented. This is the first quantitative set of experiments documenting the adiabatic expansion of a warm dense plasma on ~10- to 100-ns time scales. We also measure n_e and T_e of the degenerate plasma 200 ns after energy is deposited into thin foils by an intense relativistic electron beam.

II. COLLISIONAL HEATING AND OPTICAL MEASUREMENTS

The collisional heating process is performed by depositing the particle beam energy into the material lattice of the foil and stripping the electrons from the atom. In this case the particles inducing the collisions are relativistic electrons. Since we are operating near the minimum of the electronic stopping power (dE/dx) curve the collisional heating is not optimized [40]. The energy dissipated into these thin (100-μm) foils is 9.7 J in Ti, assuming a 1-mm radial distribution; $< 0.5\%$ of the available 2.7 kJ of particle beam energy. This is understandable because the range (penetration depth) of relativistic electrons at this kinetic energy is 2.3 cm in Ti, >200 times our foil thickness. However, it is unnecessary to use thicker foils because the energy is deposited isochorically and we will not achieve any higher temperatures with thicker foils; we will just create more Bremsstrahlung x-ray radiation scattered into our diagnostics, reducing the signal-to-noise ratio.

The current density, $J(x,y)$, is temporally resolved through a near-field OTR measurement [35–39], which is made with an ICCD camera [41]. We state near-field because we are imaging the beam distribution on the surface of the foil as shown in Fig. 2(a) rather than the far-field distribution (at ∞), in which we measure the radiation lobes with polarization. The camera shown at the top of Fig. 1 (in red) is mounted upstream of the vacuum vessel, parallel to the beam axis, and is used with a set of four mirrors to view only the forward-scattered OTR at a 20° angle on the back side of the foil. We use the near-field approach to determine the peak focus after the 20-ns rise time in the pulse, 30 ns prior to any plasma generation, as shown below. A sample shot of the peak focus is shown in Fig. 2, with a Gaussian fit to the distribution indicating that $a = 2.23$ mm and FWHM = 2.63 mm, where $a = 2\sigma$.

In addition, we simultaneously measure the generation of a target plume, indicating that an average particle beam density threshold of $\langle n_e \rangle > 10^{17}$ m^{-3} is required to generate an expanding warm dense plasma. Plume expansion measurements are made with two separate cameras. The first is a legacy PI-Max512 ICCD camera [41], capable of resolving down to 5-ns gates at a 16-bit digitization rate. The second camera is a Simacon image intensified fast-framing camera composed of 8 individual ICCDs, capable of taking 2 gated, 12-bit images each (16 total). Each ICCD is capable of resolving down to 5 ns, with 1 ns between one camera frame and the next, within a minimum window of 600 ns for all 16 images. The two cameras are mounted external to the diagnostic vacuum section shown in Fig. 1 (in blue and green). The light is reflected by a single mirror to image the upstream expansion of the plume.

The expansion of a Ti foil heated by the 1.7-kA beam pulse was measured on consecutive shots with the single-frame camera in Fig. 3(a). Fifty nanoseconds into the pulse, ionization becomes visible, the intensity begins to increase slightly, with subsequent 20-ns gates, and we see rapid expansion, ~1 mm/20 ns. However, this expansion slows down 10× in the first 100 ns, indicating that the expansion is adiabatic, like a point-source explosion [42–44]. The shock front or leading edge of the plume is compared to the similarity solution: $z(t) = \eta(Et^2/\rho_o)^{1/5}$, where η is a geometric constant, E is the energy deposited into the Ti foil (9.7 J), t is time, and ρ_o is the density of the foil (4510 kg/m^3). The rate of expansion

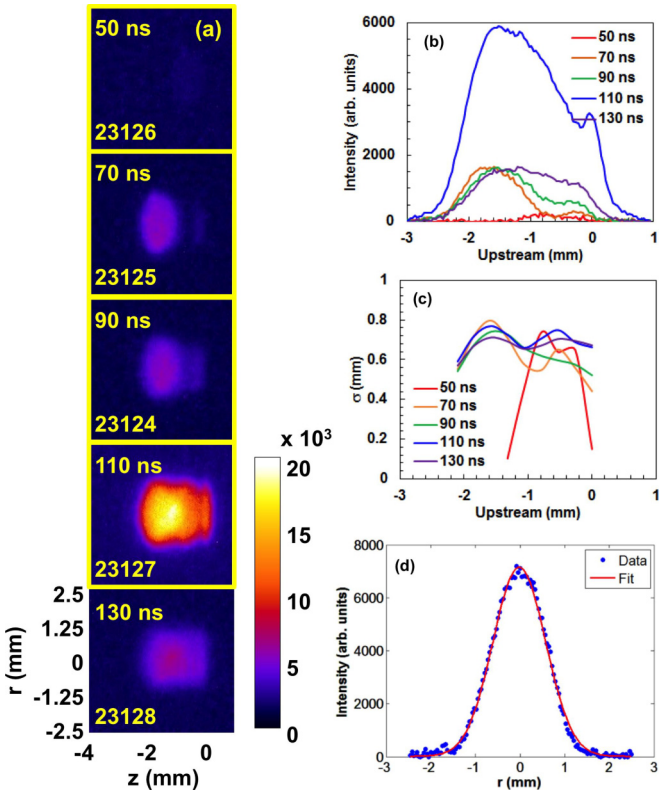

FIG. 3. (a) Twenty-nanosecond gated images of the expanding plume; the delay after the beginning of the beam pulse and the shot number are indicated. (b) Integrated intensity and axial extent of the plume images in (a). (c) Plot of σ vs the z axis for each time slice in (a). (d) Sample Gaussian fit at 2.1 mm for the 110-ns gate on shot 23127. Note that 0 is the upstream side of the target face.

of the plume $v(t)$ is simply

$$v(t) = \frac{dz(t)}{dt} = \frac{2\eta}{5}\left(\frac{E}{\rho_o}\right)^{1/5} t^{-3/5}. \quad (1)$$

As shown below, the experimental measurements we have made with two separate camera systems over multiple shots agree well with the point-source solution for adiabatic expansion. At 110 ns after the beginning of the pulse the intensity increases 5×, where the warm dense plasma begins radiating the most as shown in Fig. 3(b). After that point it continues to expand and cool off as shown by the reduced intensity. A radial profile was extracted at 250-μm intervals, providing σ vs the expansion axis [Fig. 3(c)] for each time slice in Fig. 3(a). A sample Gaussian fit at 2.1 mm for the 110-ns gate is also shown [Fig. 3(d)], indicating radial symmetry, although there is axial dependence to the expansion, which may be a characteristic of a shock.

A full expansion of Ti was examined on a single-shot basis with the fast-framing camera. Several shots were taken to determine the repeatability of the expansion rate of the visible plume with 100-ns and 1-μs gates (Fig. 4). During the first 100-ns frame the plume is about 1 mm^2. This is >2 times smaller than the total integrated size measured with the PI-Max camera in Fig. 3. Keep in mind that the sensitivity of the pixels in this camera is >10 times less than that of the PI-Max; the Simacon has 12 bits of dynamic range and the PI-Max has 16 bits. As a result of this reduced range, the gain was minimized in these images and a 5% or 10% transmission neutral density filter was used in order to measure the full dynamic nature of the expansion. In each subsequent frame for the 100-ns data set, the intensity is slightly reduced and the measured plume expansion rate decreases from 3.8 to 1.0 mm/μs over the 0.1- to 1.0-μs band [Figs. 4(a) and 4(c)]. This agrees pretty well with the similarity solution in Eq. (1), although there are a few outliers. At these time scales (>100 ns) the plasma has expanded out of the warm dense phase into a moderately coupled, $\Gamma \sim 0.1$, and degenerate, $\theta > 10^2$, plasma regime, where we are referring to the Coulomb coupling and the degeneracy (θ = thermal energy/Fermi energy). At this point we approximate the state of the plasma as an ideal gas; we are currently evaluating the correct EOS for modeling the heating and expansion of these plasmas [30–32].

The mean expansion speed for the 100-ns data set is ~1.5 mm/μs, which corresponds to a calculated Ti temperature of 0.74 eV, target pressure of 6.7×10^4 bar, and hydrodynamic disassembly time of 31.7 ns from solid density,

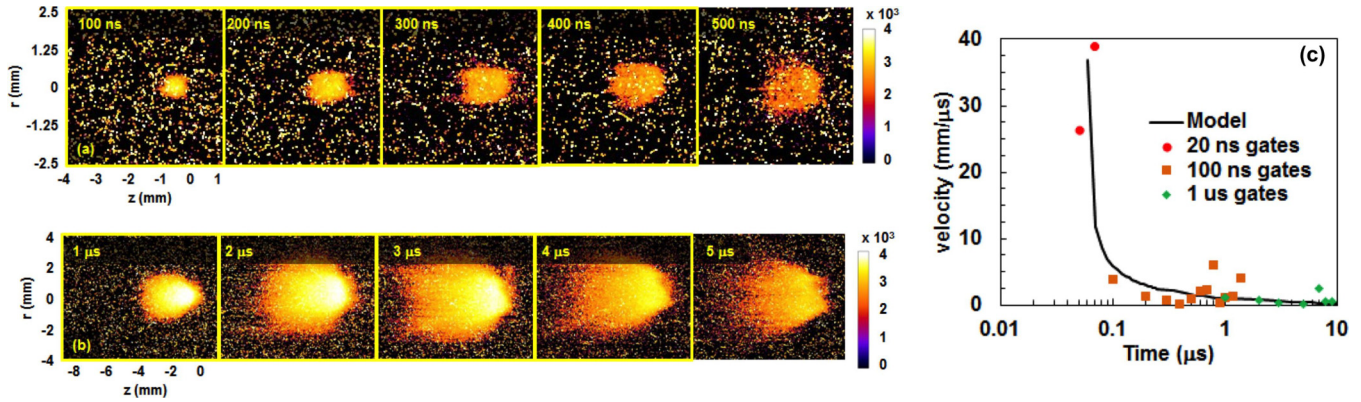

FIG. 4. (a) One hundred–nanosecond gated images of the expanding plume; the delay after the beginning of the pulse is indicated, and the shot number is 23103. (b) One-microsecond gated images of the expanding plume and gate with respect to the beginning of the pulse; shot number 23105 (note the scale differences). Images are shown at log scale to indicate full expansion. (c) Velocity profile of multiple 20-ns (red circles), 100-ns (orange squares), and 1-μs (green diamonds) gated images from the PI-Max512 and Simacon fast-framing cameras. The black line represents the point-source solution from Eq. (1).

TABLE I. Measured and calculated plasma parameters based on the collisional stopping power (dE/dx) of a 20-MeV electron beam in a radius r. Calculated values were obtained assuming an ideal gas. Measured values are followed by a superscript "m."

r (mm)	T_e (eV)	P (Mb)	C_s (mm/μs)	t_{hydro} (ns)
0.94	1.24^{m}	0.112	2.04	24.5
1.20	0.74	0.067	1.57^{m}	31.7
1.80	0.30	0.027	1.00	50^{m}

as shown in the second row of data in Table I. The measured values are listed in the table and the remaining unknown values are roughly approximated assuming an ideal gas. The values can be computed from the collisional stopping power dE/dx of a 20-MeV electron beam into 100-μm-thick Ti foil, where $dE/dx = 1.584$ MeV-cm^2/g. The change in temperature ΔT (K) is

$$\Delta T = \frac{q\frac{dE}{dx}}{\pi r^2 C}, \tag{2}$$

where q is the total electron charge deposited by the electron beam, which is $\sim$140 μC, r is the beam radius, and C (J/g-K) is the specific heat of the material. The target plasma pressure P (N/m^2) can be calculated from the electron density n_e (m^{-3}) and temperature (eV), $P = n_e k_B T$, where k_B is the Boltzmann constant and the temperature conversion of 11 604 K/eV is also required. The sound-speed expansion of the warm dense plasma is estimated by $C_s = (\gamma Z P/\rho_o)^{1/2}$, where γ is the adiabatic index or isentropic expansion factor ($\gamma = C_p/C_v$), which for our case, a monoatomic metallic plasma, is 5/3. Z is the charge state of the plasma and ρ_o is the solid density of the target material. Finally, the hydrodynamic disassembly time for expansion on two sides is estimated as $t_{\text{hydro}} = \Delta z/2C_s$, where Δz is the target thickness. The plume expands to much larger distributions at a much slower rate when measured with 1-μs gates [Figs. 4(b) and 4(c)]. These 1-μs images indicate an overlap with the 100-ns data set, showing a reduced expansion rate, from 1.0 to 0.3 mm/μs, over the 1.0- to 10-μs band.

Visible spectroscopy measurements were conducted with a pair of Princeton Instruments Acton spectrometers [45] and PI-Max4 ICCDs [41]. More specific details of this diagnostic are outlined in [46]. The light from the warm dense plasma is coupled into the linear fiber array with a 130-mm lens as shown in Fig. 1. Figures 5(a)–5(c) illustrate a high-resolution

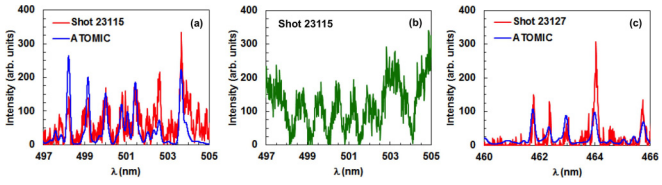

FIG. 5. Measured Ti-I spectra over a 200-ns gate, indicating (a) emission and (b) absorption for shot 23115 over the 496- to 506-nm band and (c) emission for shot 23127 over the 454- to 466-nm band. The ATOMIC fit calculation is shown in blue for comparison.

measurement (1800 G/mm) of the Ti spectrum measured over a 200-ns period, 300 ns after the beginning of the pulse (or 200 ns after the pulse has ended), on two separate shots. Lower intensity emission has been observed 100 ns earlier. Each shot provided a bandwidth of 8–9 nm and a resolution of < 0.12 Å, and the emitted lines are only Ti-I lines. On shot 23115 we measured both emitted and absorbed spectra [Figs. 5(a) and 5(b)] on two separate fibers, which appeared to be mirror images of one another in intensity. On shot 23127 we measured additional emission spectra in a lower band.

The Los Alamos suite of atomic structure and collision codes [48] was used to generate atomic energy levels, wave functions, and transition probabilities utilizing the semirelativistic CATS [49,50] atomic structure code, available NIST values [51], and the multipurpose ionization code GIPPER [48,52]. Plasma modeling calculations were then performed for the neutral, singly ionized, and doubly ionized species of Ti using the Los Alamos ATOMIC code [53,54] and the atomic data generated from CATS and GIPPER. ATOMIC was run in local-thermodynamic-equilibrium mode, which should be a good approximation for the plasma conditions considered here [47,55]. The emission produced from these modeling calculations is presented in Figs. 5(a) and 5(c). Every line measured in both wavelength bands is reproduced by the calculations, and the best-fit estimates for the temperature and density result in $T_e = 1.25$ eV and $n_e = 3 \times 10^{17}$ cm^{-3}. This indicates that the average density has expanded 5 orders below ρ_o, 200 ns after energy deposition.

This measured T_e is used to estimate the heated radius, P, C_s, and t_{hydro} at solid density as shown in the first row of data in Table I, indicating a slightly better deposition of energy than estimated from the expansion images. A comparison to $t_{\text{hydro}} = 50$ ns, based on the measurements in Fig. 3, is also shown in the bottom row of data in Table I to illustrate the colder $T_e = 0.30$ eV. A better spectral fit could be obtained by performing a detailed radiation transport model that incorporates the spatial temperature and density distribution and the opacity of each spectral line [56]. However, this requires a time-resolved density gradient measurement and a detailed hydro model, which we are currently developing.

III. CONCLUSIONS

We confirmed that we produce a large volume of adiabatically expanding warm dense plasma through isochoric heating with an electron beam, $\langle n_e \rangle > 10^{17}$ m^{-3}, $< 10^{10}$ of solid-density Ti. We developed a spatial and temporal profile of the expanding plasma off the target surface, which agrees well with the point-source solution and for multiple diagnostics. The spatial distributions are extremely reproducible for identical incoming beam parameters. Visible expansion of the plume does not begin until $\sim$50 ns into the beam pulse and the peak intensity is observed near the end of energy deposition.

Visible emission and absorption lines of Ti-I are only observed $>$100–200 ns after energy is deposited, once the plasma has adiabatically expanded and cooled into a degenerate plasma. The Los Alamos National Laboratory ATOMIC

code is able to reproduce the spectra to first order and provide a measured $T_e = 1.25$ eV and $n_e = 3 \times 10^{17}$ cm^{-3}, which indicate a slightly higher temperature than was estimated by the expansion measurements with the ICCD cameras. This confirms that we are not measuring the EOS in the warm dense phase. We are still deploying additional density and x-ray diagnostics to characterize the temperature and density of the WDM at early times (<100 ns). We are also evaluating the correct EOS for modeling the heating and expansion of these plasmas. In addition, we wish to measure the expansion velocity of the foil and a disassembly time with a PDV probe. Each of these should help provide a conclusive measurement of how long the warm dense phase lasts with this heating method and a map of the EOS across the density range of $10^{16} < n_e\ (\text{cm}^{-3}) < 10^{23}$.

ACKNOWLEDGMENTS

We would like to thank M. Berninger, C. A. Ekdahl, and M. E. Schulze for technical discussions. We would like to take the opportunity to thank Don Roeder, Valerie Fatherley, Anthony Chavez, and Sharon Dominguez for their manufacturing and design support. We also would like to thank the operators, technicians, students, and engineers Sam Snider, Jules Carson, Josh Esquibel, Geronimo Gonzalez, Robbie Brooks, Melissa Reed, Tim McCurdy, Rudy Valdez, Armando Martinez, Tim Rushenberg, Nick Ramey, and Travis Weaver for their continued support. This work was supported by the National Nuclear Security Administration of the U.S. Department of Energy under Contract No. DE-AC52-06NA25396.

[1] A. L. Kritcher *et al.*, Phys. Plasmas **16**, 056308 (2009).
[2] A. L. Kritcher, P. Neumayer, C. R. D. Brown, P. Davis, T. Döppner, R. W. Falcone, D. O. Gericke, G. Gregori, B. Holst, O. L. Landen, H. J. Lee, E. C. Morse, A. Pelka, and R. Redmer, Phys. Rev. Lett. **103**, 245004 (2009).
[3] L. B. Fletcher, A. L. Kritcher, A. Pak, T. Ma, T. Döppner, C. Fortmann, L. Divol, O. S. Jones, O. L. Landen, H. A. Scott, J. Vorberger, D. A. Chapman, D. O. Gericke, B. A. Mattern, G. T. Seidler, G. Gregori, R. W. Falcone, and S. H. Glenzer, Phys. Rev. Lett. **112**, 145004 (2014).
[4] A. Levy, P. Audebert, R. Shepherd, J. Dunn, M. Cammarata, O. Ciricosta, F. Deneuville, F. Dorchies, M. Fajardo, C. Fourment, D. Fritz, J. Fuchs, J. Gaudin, M. Gauthier, A. Graf, H. J. Lee, H. Lemke, B. Nagler, J. Park, O. Peyrusse, A. B. Steel, S. M. Vinko, J. S. Wark, G. O. Williams, D. Zhu, and R. W. Lee, Phys. Plasmas **22**, 030703 (2015).
[5] J. Cihelka, L. Juha, J. Chalupský, F. B. Rosmej, O. Renner, K. Saksl, V. Hájková, L. Vyšin, E. Galtier, R. Schott, A. R. Khorsand, D. Riley, T. Dzelzainis, A. J. Nelson, R. W. Lee, P. A. Heimann, B. Nagler, S. Vinko, J. Wark, T. Whitcher, S. Toleikis, T. Tschentscher, R. Faustlin, H. Wabnitz, S. Bajt, H. Chapman, J. Krzywinski, R. Sobierajski, D. Klinger, M. Jurek, J. Pelka, S. Hau-Riege, R. A. London, J. Kuba, N. Stojanovic, K. Sokolowski-Tinten, A. J. Gleeson, M. Störmer, J. Andreasson, J. Hajdu, B. Iwan, and N. Timneanu, Proc. SPIE **7361**, 73610P (2009).
[6] A. L. Kritcher, T. Doeppner, D. Swift, J. Hawreliak, J. Nilsen, J. Hammer, B. Bachmann, G. Collins, O. Landen, C. Keane, S. Glenzer, S. Rothman, D. Chapman, D. Kraus, and R. W. Falcone, J. Phys.: Conf. Ser. **688**, 012055 (2016).
[7] T. Ao, E. C. Harding, J. E. Bailey, R. W. Lemke, M. P. Desjarlais, S. B. Hansen, I. C. Smith, M. Geissel, A. Maurer, J. Reneker, D. Romero, D. B. Sinars, G. A. Rochau, and J. F. Benage, High Energy Density Phys. **18**, 26 (2016).
[8] P. F. Knapp, S. A. Pikuz, T. A. Shelkovenko, D. A. Hammer, and S. B. Hansen, Phys. Plasmas **19**, 056302 (2012).
[9] N. A. Tahir *et al.*, Laser Part. Beams **22**, 485 (2004).
[10] A. Tauschwitz, J. A. Maruhn, D. Riley, F. B. Rosmej, S. Borneis, A. Tauschwitz, and K. Witte, J. Phys.: Conf. Ser. **112**, 032074 (2008).
[11] P. A. Ni, M. I. Kulish, V. Mintsev, D. N. Nikolaev, V. Ya. Ternovoi, D. H. H. Hoffmann, S. Udrea, A. Hug, N. A. Tahir, and D. Varentsov, Laser Part. Beams **26**, 583 (2008).
[12] J. E. Coleman, Ph.D. thesis, University of California, Berkeley, 2008.
[13] F. M. Bieniosek, J. J. Barnard, A. Friedman, E. Henestroza, J. Y. Jung, M. A. Leitner, S. Lidia, B. G. Logan, R. M. More, P. A. Ni, P. K. Roy, P. A. Seidl, and W. L. Waldron, J. Phys.: Conf. Ser. **244**, 032028 (2010).
[14] P. A. Ni, F. M. Bieniosek, E. Henestroza, and S. M. Lidia, Nucl. Instrum. Methods Phys. Res., Sec. A **733**, 12 (2014).
[15] P. A. Seidl, A. Persaud, W. L. Waldron, J. J. Barnard, R. C. Davidson, A. Friedman, E. P. Gilson, W. G. Greenway, D. P. Grote, I. D. Kaganovich, S. M. Lidia, M. Stettler, J. H. Takakuwa, and T. Schenkel, Nucl. Instrum. Methods Phys. Res., Sec. A **800**, 98 (2015).
[16] P. A. Seidl, J. J. Barnard, R. C. Davidson, A. Friedman, E. P. Gilson, D. Grote, Q. Ji, I. D. Kaganovich, A. Persaud, W. L. Waldron, and T. Schenkel, J. Phys.: Conf. Ser. **717**, 012079 (2016).
[17] P. A. Seidl (private communication).
[18] A. Pelka, G. Gregori, D. O. Gericke, J. Vorberger, S. H. Glenzer, M. M. Günther, K. Harres, R. Heathcote, A. L. Kritcher, N. L. Kugland, B. Li, M. Makita, J. Mithen, D. Neely, C. Niemann, A. Otten, D. Riley, G. Schaumann, M. Schollmeier, An. Tauschwitz, and M. Roth, Phys. Rev. Lett. **105**, 265701 (2010).
[19] W. Bang, B. J. Albright, P. A. Bradley, D. C. Gautier, S. Palaniyappan, E. L. Vold, M. A. Santiago Cordoba, C. E. Hamilton, and J. C. Fernández, Sci. Rep. **5**, 14318 (2015).
[20] W. Bang, B. J. Albright, P. A. Bradley, E. L. Vold, J. C. Boettger, and J. C. Fernandez, Phys. Rev. E **92**, 063101 (2015).
[21] M. Gittings, R. Weaver, M. Clover, T. Betlach, N. Byrne, R. Coker, E. Dendy, R. Hueckstaedt, K. New, W. R. Oakes, D. Ranta, and R. Stefan, Comput. Sci. Disc. **1**, 015005 (2008).
[22] S. P. Lyon and J. D. Johnson, *Sesame: The Los Alamos National Laboratory Equation of State Database*, Los Alamos National Laboratory Report No. LA-UR-92-3407 (Los Alamos National Laboratory, Los Alamos, NM, 1992).
[23] G. Hairapetian, P. Davis, C. E. Clayton, C. Joshi, S. C. Hartman, C. Pellegrini, and T. Katsouleas, Phys. Rev. Lett. **72**, 2403 (1994).
[24] G. Hairapetian, P. Davis, C. E. Clayton, C. Joshi, C. Pellegrini, and T. Katsouleas, Phys. Plasmas **2**, 2555 (1995).
[25] C. Joshi, B. Blue, C. E. Clayton, E. Dodd, C. Huang, K. A. Marsh, W. B. Mori, S. Wang, M. J. Hogan, C. O'Connell,

R. Siemann, D. Watz, P. Muggli, T. Katsouleas, and S. Lee, Phys. Plasmas **9**, 1845 (2002).
[26] C. Vermare, H. A. Davis, D. C. Moir, and T. P. Hughes, Phys. Plasmas **10**, 277 (2003).
[27] S. Sampayan, R. Buckles, G. Caporaso, F. C. Chambers, Y-J Chen, S. Falabella, F. Goldin, G. Guethlein, D. Ho, M. Heino, T. Houck, E. Lauer, J. McCarrick, R. Neurath, P. Pincosy, R. Richardson, D. Sanders, and J. Weir, in *Proceedings of the Particle Accelerator Conference, Chicago, 2001* (IEEE, New York, 2001), p. 330.
[28] D. R. Welch and T. P. Hughes, Laser Part. Beams **16**, 285 (1998).
[29] B. V. Oliver, D. R. Welch, and T. P. Hughes, *Beam-Target Interactions in Single- and Multi-Pulse Radiography*, MRC/ABQ-R-1909 Report (Mission Research Corp., Albuquerque, NM, 1999).
[30] M. J. Berninger and T. Kwan (private communication).
[31] M. L. Klasky (private communication).
[32] D. R. Welch and C. L. Miller (private communication).
[33] J. E. Coleman, D. C. Moir, C. A. Ekdahl, J. B. Johnson, B. T. McCuistian, G. W. Sullivan, and M. T. Crawford, Phys. Rev. ST Accel. Beams **17**, 030101 (2014).
[34] J. E. Coleman, C. A. Ekdahl, D. C. Moir, G. W. Sullivan, and M. T. Crawford, Phys. Rev. ST Accel. Beams **17**, 092802 (2014).
[35] L. Wartski, S. Roland, J. Lasalle, M. Bolore, and G. Filippi, J. Appl. Phys. **46**, 3644 (1975).
[36] C. B. Reid, Master's thesis, Naval Postgraduate School, Monterey, CA, 1990.
[37] B. Gitter, CAA Tech. Note 24 (1992).
[38] R. B. Fiorito and D. W. Rule, AIP Conf. Proc. **319**, 21 (1994).
[39] P. Karataev, A. Aryshev, S. Boogert, D. Howell, N. Terunuma, and J. Urakawa, Phys. Rev. Lett. **107**, 174801 (2011).
[40] See physics.nist.gov/cgi-bin/Star/e_table.pl for information about *dE/dx*.
[41] See http://www.princetoninstruments.com/products/imcam/pimax/ for information about PI-Max cameras.
[42] H. A. Bethe, K. Fuchs, J. O. Hirschfelder, J. L. Magee, R. E. Peierls, and J. von Neumann, in *BLAST WAVE*, Los Alamos Report LA-2000 (Los Alamos National Laboratory, Los Alamos, NM, 1947), chap. 2.
[43] G. I. Taylor, Proc. R. Soc. A **201**, 159 (1950).
[44] G. I. Taylor, Proc. R. Soc. A **201**, 175 (1950).
[45] See http://www.princetoninstruments.com/products/spec/actonseries/ for information about Acton spectrometers.
[46] J. E. Coleman, Rev. Sci. Instrum. **87**, 123113 (2016).
[47] J. Colgan, E. J. Judge, D. P. Kilcrease, and J. E. Barefield II, Spectrochim. Acta B **97**, 65 (2014).
[48] C. J. Fontes, H. L. Zhang, J. Abdallah Jr, R. E. H. Clark, D. P. Kilcrease, J. Colgan, R. T. Cunningham, P. Hakel, N. H. Magee, and M. E. Sherrill, J. Phys. B **48**, 144014 (2015).
[49] R. D. Cowan, *The Theory of Atomic Structure and Spectra* (University of California Press, Berkeley, 1981).
[50] J. Abdallah, R. E. H. Clark, and R. D. Cowan, *CATS: Cowan Atomic Structure Code*, Manual No. LA 11436-M-I (Los Alamos National Laboratory, Los Alamos, NM, 1988).
[51] A. Kramida, Y. Ralchenko, and J. Reader, *NIST ASD Team 2014 NIST Atomic Spectra Database v. 5.2* (NIST, Gaithersburg, MD, 2014). See http://physics.nist.gov/PhysRefData/ASD/lines_form.html for information about documented Ti-I lines.
[52] R. E. H. Clark, J. Abdallah Jr., and J. B. Mann, Astrophys. J. **381**, 597 (1991).
[53] N. H. Magee, J. Abdallah, J. Colgan, P. Hakel, D. P. Kilcrease, S. Mazevet, M. Sherrill, C. J. Fontes, and H. L. Zhang, in *14th Topical Conference on Atomic Processes in Plasmas*, edited by J. S. Cohen, S. Mazevet, and D. P. Kilcrease (American Institute of Physics, Melville, NY, 2004), pp. 168–179.
[54] P. Hakel, M. E. Sherrill, S. Mazevet, J. Abdallah Jr., J. Colgan, D. P. Kilcrease, N. H. Magee, C. J. Fontes, and H. L. Zhang, J. Quant. Spectrosc. Rad. Transfer **99**, 265 (2006).
[55] R. W. P. McWhirter, *Plasma Diagnostic Techniques* (Academic Press, New York, 1965).
[56] P. Hakel, Comput. Phys. Commun. **207**, 415 (2016).